Journal of Materials Chemistry A

PAPER

View Article Online
View Journal | View Issue

Published on 09 April 2014. Downloaded by Xian Jiaotong University on 04/11/2015 03:22:23.

Cite this: J. Mater. Chem. A, 2014, 2, 8790

Bioinspired underwater superoleophobic surface with ultralow oil-adhesion achieved by femtosecond laser microfabrication†

Jiale Yong, Feng Chen,* Qing Yang, Dongshi Zhang, Umar Farooq, Guangqing Du and Xun Hou

Received 14th March 2014
Accepted 9th April 2014

DOI: 10.1039/c4ta01277a

www.rsc.org/MaterialsA

Femtosecond laser microfabrication has been recently utilized in interface science to modify the liquid wettability of solid surfaces. In this paper, a silicon surface with hierarchical micro/nanostructure is fabricated by a femtosecond laser. Similar to fish scales, the laser-induced surface shows superhydrophilicity in air and superoleophobicity underwater. The oil contact angles can reach up to 159.4 ± 1° and 150.3 ± 2°, respectively, for 1,2-dichloroethane and chloroform droplets in water. In addition, the surface exhibits ultralow oil-adhesion. In the oil–water–solid three-phase system, water can be trapped in the hierarchical rough structure and form a repulsive oil layer according to the extended Cassie's theory. The contact area between the as-prepared surface and oil droplets is significantly reduced, resulting in superoleophobicity and ultralow oil-adhesion in water. In addition, as a potential application, the working principle diagram of preventing blockage ability of underwater superoleophobic pipes is propounded.

1. Introduction

Wettability is a very important property of solid surfaces; it is governed by both the geometrical microstructure and the chemical composition of the materials.[1–9] A superhydrophobic surface, displaying a water contact angle (WCA) greater than 150°, was initially observed in natural materials such as lotus leaf.[10,11] The lotus leaf surface is found to be completely covered by many micro/nanoscale hierarchical papillae and an additional layer of hydrophobic wax crystals.[12–16] The combined action can minimize the real contact area between the surface and the droplet, leading to great enhancement of superhydrophobicity. Inspired by the lotus leaf, artificial superhydrophobic surfaces have been designed in large numbers and are widely used in many fields, for instance in the areas of surface self-cleaning, marine coating, preventing the adhesion of snow, fog and raindrops to window surfaces and reducing flow resistance in microfluidic channels.[17–23] Oil, another common liquid in our daily life, is recently most often selected as a research object to investigate the interface of solid and liquid.[24–31] In studying a superhydrophobic surface, we found that the superoleophobicity can be characterized by an oil contact angle (OCA) larger than 150°.

It is well known that fish can swim freely under water and keep their scales clean even in oil-polluted water following an oil spill.[32,33] Recently, Jiang *et al.* revealed that this remarkable ability is ascribed to the special underwater superoleophobicity of fish scales.[34,35] The combination of the hierarchical rough structures and hydrophilic chemistry of fish scales gives rise to their underwater superoleophobicity. According to Cassie's theory, an air layer can be trapped in the water–solid interface when a water droplet is placed on a rough solid surface that has low surface energy in an air environment.[36] It provides a water–air–solid interface that reduces the contact area between water and solid, leading to a high WCA. Air is an ideal water-repellent material because a small water droplet suspended in air is spherical.[37] For the same reason, water is an excellent oil-repellent material. Similar to the role of an air layer for achieving superhydrophobicity, if water fills in between the hierarchical rough structures of a solid surface, a water layer can form at the oil–solid interface. The water layer can improve oleophobicity at the oil–water–solid interface, which may provide the possibility for fabricating underwater superoleophobic surfaces.[34,35] Taking inspiration from these findings, many underwater superoleophobic materials have been prepared.[27] These novel materials show some amazing practical applications, such as preventing blockage, bio-adhesion, microfluidic technology, and oil–water separation.[38–43] However, most reported methods used to fabricate underwater superoleophobic surfaces generally require complex fabrication processes, have tight restrictions on materials, and lack

State Key Laboratory for Manufacturing System Engineering & Key Laboratory of Photonics Technology for Information of Shaanxi Province, School of Electronics & Information Engineering, Xi'an Jiaotong University, Xi'an, 710049, P. R. China. E-mail: chenfeng@mail.xjtu.edu.cn

† Electronic supplementary information (ESI) available. See DOI: 10.1039/c4ta01277a

This journal is © The Royal Society of Chemistry 2014

Published on 09 April 2014. Downloaded by Xian Jiaotong University on 04/11/2015 03:22:23.

flexibility. A versatile and simple way to realize underwater superoleophobicity has yet to be found in the published literature.

In recent years, micromachining by femtosecond laser has been utilized in interface science to modify the liquid wettability of solid surfaces.[44–51] This technology has many distinct advantages, such as a negligible heat-affected zone, precise ablation threshold and high resolution.[44,50] Moreover, this method can be applied to a wide variety of materials such as metals, glasses, ceramics and polymers.[52–55] A two-scale rough microstructure can be easily built by femtosecond laser scanning. Controlled by a computer, femtosecond laser micromachining provides a quick and efficient prototyping means that can control the processing position precisely, without the need for expensive masks and a clean room. Various patterns can be realized that exhibit unique wetting properties. Although this technology has been a great success in achieving superhydrophobic surfaces, to the best of our knowledge, the fabrication of superoleophobic surfaces *via* a femtosecond laser is still scarce.

In this paper, we present an effective method for preparation of an underwater superoleophobic surface by femtosecond laser microfabrication on silicon in an ambient environment. After irradiating by femtosecond laser pulses through a line-by-line and serial scanning process, the sample surface shows a micro/nanoscale hierarchical spike forest structure. The hierarchical surface of high roughness exhibits extreme underwater superoleophobicity, with OCAs greater than 150° for 1,2-dichloroethane and chloroform droplets in water. The adhesion between the as-prepared surface and oil droplet is very low; the oil droplets can move easily even when the surface is only slightly tilted. In addition, as a potential application, we attempt to put forward a working principle diagram of an underwater superoleophobic surface that prevents blockage caused by oil pollution.

2. Experimental section

The micro/nanoscale hierarchical structure was prepared by femtosecond laser irradiation in air on a flat silicon surface through a line-by-line and serial scanning process. The schematic of the experimental setup was shown in our previous work.[45–51] A single crystal p-type Si (100) wafer with thickness of 0.5 mm was used. The sample was mounted on a motorized x–y–z translation stage controlled by a computer and then irradiated by a regenerative amplified Ti:sapphire laser system (center wavelength: 800 nm; pulse duration: 50 fs; repetition: 1 kHz) (CoHerent, Libra-usp-1K-he-200). The Gaussian laser beam was focused by a microscope objective lens (20×, NA = 0.45, Nikon) on the front side of the sample. The laser energy was 20 mW, and the scanning speed was 2 mm s^{-1}. The interval of adjacent laser scanning lines was set at 2 μm. Since the laser repetition rate was 1 kHz, the adjacent distance of laser pulse focuses was 2 μm. Following the irradiation process, the sample was successively cleaned by acetone, alcohol, and deionized water in an ultrasonic bath for 10 minutes each time.

The morphology of the as-prepared surfaces irradiated by a femtosecond laser was characterized by a JSM-7000F scanning electron microscope (SEM, JEOL, Japan). The contact angles of an 8 μL water or oil droplet on the surface were measured by a JC2000D4 contact-angle system (POWEREACH, China). In the water contact angle test, the sample was placed on a sample stage. In the underwater oil contact angle test, the sample was put in a homemade sink filled with deionized water. For detecting oils, 1,2-dichloroethane ($C_2H_4Cl_2$) and chloroform ($CHCl_3$) were used. The average values were obtained by measuring five different points on the same surface. The adhesion between the as-prepared surface and oil droplets in water was investigated by the contact-angle system and a charge-coupled device (CCD) camera system to take photographs at 25 frames per second.

3. Results and discussion

Fig. 1 shows typical SEM images of the femtosecond laser-induced structure. The morphology is characterized by a self-organized conical spike forest with period of 10 μm. Each spike is decorated with tens or a few hundreds of nanometer-sized protrusions. The micro/nanoscale hierarchical structure is highly uniform. The formation of this structure is considered to evolve from the microscale ridges.[37,51,56,57] The average diameter of the periodic conical spikes is about 6 μm, and the height is 2.9 μm (Fig. 1d). Every conical spike is surrounded by four microscale holes. The average diameter and depth of the holes are about 8 and 4.6 μm, respectively. As a result, the distance from the top of the spikes to the bottom of the holes can reach up to 7.5 μm, resulting in a significant increase in the overall roughness. The surface roughness (R_a) is about 2.46 μm. This hierarchical rough structure is helpful for achieving superhydrophilicity in air and superoleophobicity in water.

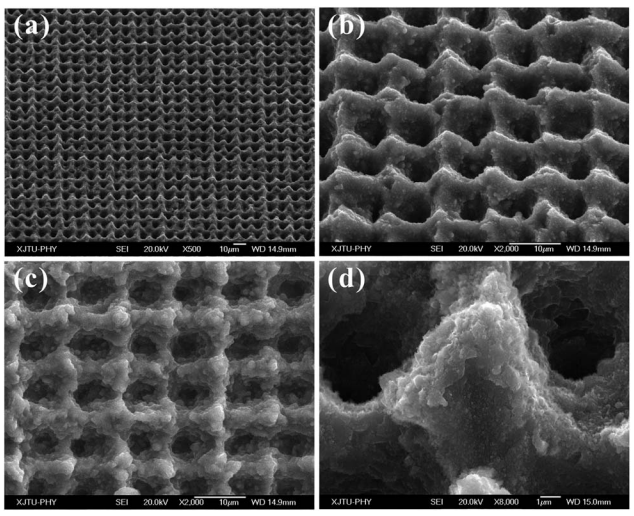

Fig. 1 Typical SEM images of the structure irradiated by femtosecond laser. (a) 45° tilted view SEM image. (b) Higher resolution 45° tilted view SEM image. (c) Top view SEM image. (d) High magnification SEM image of a single spike decorating with nanoscale protrusions.

Published on 09 April 2014. Downloaded by Xian Jiaotong University on 04/11/2015 03:22:23.

Previous studies have shown that the superhydrophilicity of a solid surface in air is crucial for realizing superoleophobicity in water.[27,34,35] When a water droplet is placed on a flat silicon surface in air, the WCA is about 60° (Fig. 2a). In water, the shape of oil droplet is nearly half-sphere alike. The OCA is 124.6 ± 1° for an oil (1,2-dichloroethane) droplet, indicating the silicon wafer behaves as an commonly oleophobic surface in water (Fig. 2c). After femtosecond laser irradiation, the as-prepared surface shows superhydrophilicity in air. When a water droplet is placed on the as-prepared surface, it can spread quickly, resulting in a contact angle of nearly 4° (Fig. 2b). Fig. 2d shows the image of an 8 μL oil droplet lying on the laser-induced surface in water. The oil droplet is approximately spherical in shape, and the OCA is as high as 159.4 ± 1°, indicating underwater superoleophobicity.

The average distance (D) of laser pulse focuses, which is determined by the scanning speed and interval of adjacent laser scanning lines, is a crucial machining parameter in our experiment. A detailed definition of D can be found by consulting our previous work.[48] Fig. 3 shows the dependence of the OCA on D. It can be seen that the OCA slowly decreases from 159.4 ± 1° to 156.7 ± 2.7° as D increases from 2 μm to 25 μm. A higher D has not been tested because it might damage the equipment. Clearly, this fluctuation is negligible and all the OCAs are higher than 150°, indicating that underwater superoleophobicity can be realized in a wide technology parameter range. The result shows that femtosecond laser microfabrication is a useful and effective method for producing underwater superoleophobic surfaces.

The underwater oil-adhesion of the femtosecond laser structured surface was investigated by three usual means. As seen in Fig. 4a and Movie S1 in ESI,† a 6 μL oil (1,2-dichloroethane) droplet was first suspended on a microsyringe and then slowly lowered. After the as-prepared surface made contact with the oil droplet, the microsyringe was lifted up. Interestingly, the suspending oil droplet had difficulty falling on the structured surface; that is, in comparison with the large droplet, the surface adhesion was negligible even though the droplet was severely deformed by the downward pushing force produced during microsyringe decline. As the microsyringe was moved upward, the droplet would depart from the sample and be taken away. During the entire contacting and leaving process, the oil droplet kept a nearly spherical shape at all times, and the oil droplet could be transferred without loss, showing an ultralow oil-adhesion between the as-prepared surface and the oil droplet in water. The oil droplet could detach from the microsyringe and fall on the sample under gravitation alone until the oil volume reached 8 μL. A similar process is described in Fig. 4b and Movie S2 in ESI.† An oil droplet was dragged by the needle tip of microsyringe freely along the as-prepared surface. There was also no oil loss during the oil droplet's motion. The low oil adhesion can be easily concluded by following the process in Fig. 4a.

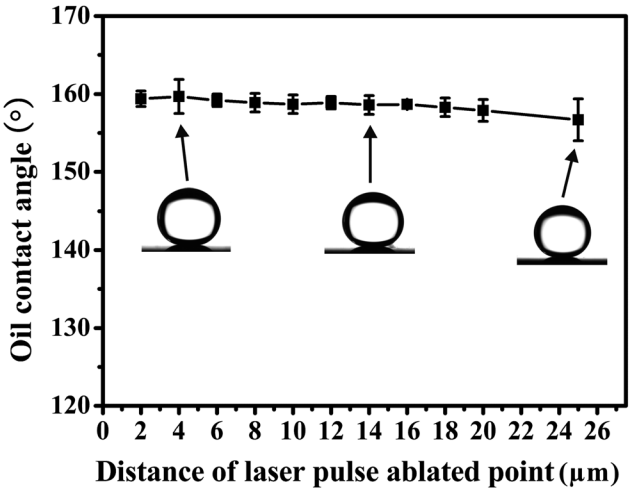

Fig. 3 Dependence of the oil contact angle on the distance of laser pulse focuses.

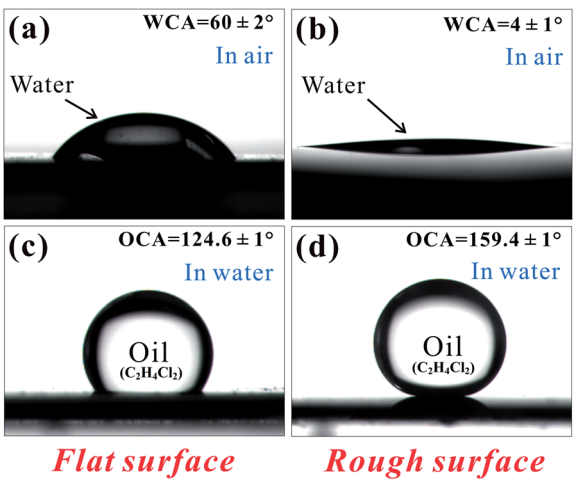

Fig. 2 Comparison of the wetting properties of the surface before and after femtosecond laser treatment. (a and b) Shapes of a water droplet on the (a) flat surface and (b) rough surface in air, respectively. (c and d) Shapes of a 1,2-dichloroethane droplet on the (c) flat surface and (d) rough surface in water, respectively.

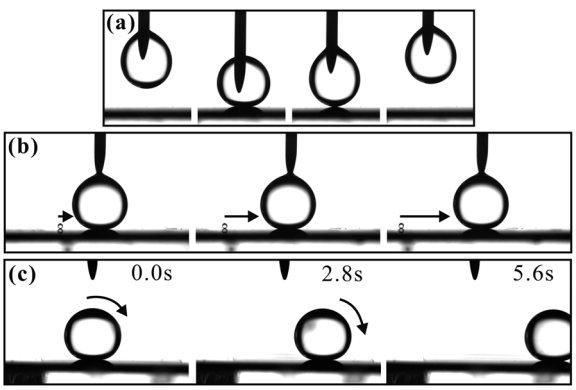

Fig. 4 Oil-adhesion of the femtosecond laser structured surface. (a) Photographs of a 6 μL oil droplet contacting and leaving with the laser-induced surface. (b) Pulling an oil droplet on the laser-induced surface. The surface was marked by location with an ultra-small liquid droplet (starting point of the black arrow) by a spraying method before the experiment. (c) Time sequence of snapshots of an oil droplet rolling on the 0.5° tilted surface. 1,2-Dichloroethane was used as the test oil.

This journal is © The Royal Society of Chemistry 2014

Published on 09 April 2014. Downloaded by Xian Jiaotong University on 04/11/2015 03:22:23.

The oil adhesion can also be accurately assessed by the sliding behavior of an oil droplet. Interestingly, experimental results show that the oil droplet can move very easily even when the as-prepared surface is only slightly tilted or shaken. Fig. 4c shows a time sequence of snapshots of an oil droplet rolling on a 0.5° tilted structured surface, indicating an ultralow adhesion between the laser-induced surface and oil droplet in water (Movie S3 in ESI†). Previously, surfactant solutions were traditionally used to reduce the adhesive force between oil droplets and solid surfaces, but these chemical substances are potentially contaminations in living environments.[34] In our experiment, the low oil-adhesion is highly dependent on the micro/nanostructures, which are considered to be environmentally friendly, instead of on surfactants. Both the high OCA and the ultralow oil-adhesion demonstrate that the as-prepared surface has an outstanding character of underwater superoleophobicity; the dual-scale hierarchical structure is very important to enhance the oleophobicity of the solid surface.

The underwater superoleophobicity and ultralow oil-adhesion can also be observed in the case of a chloroform droplet. Fig. 5a shows the shape of a chloroform droplet on the flat surface in water with an OCA of 107.7 ± 1°. After femtosecond laser irradiation, the OCA increases significantly, and its value reaches 150.3 ± 2° (Fig. 5b). The OCA has thus met the requirement of superoleophobicity. When a chloroform droplet was placed on a 1° tilted structured surface, it would instantly roll off under gravity, as shown in Fig. 5c and Movie S4 in the ESI.† The sliding angle is very low, as well as the oil-adhesion between the laser-induced surface and chloroform droplet in water.

To thoroughly understand the underwater superoleophobicity of the femtosecond laser-structured surface, a potential mechanism that explains the oil contact angles was postulated. In air, the wettability of the solid surface is generally estimated by the contact angle according to Young's equation.[27,34,35] Although the equation was originally applied to a liquid droplet on a solid surface in air, it can be extended to a liquid droplet on a solid surface in the presence of a second liquid. For example, in the oil–water–solid three-phase system (Fig. 6a), the OCA on a flat surface can be expressed by modified Young's equation:[27,34,35]

$$\cos\theta_{ow} = \frac{\gamma_{oa}\cos\theta_o - \gamma_{wa}\cos\theta_w}{\gamma_{ow}} \quad (1)$$

where γ_{oa}, γ_{wa}, and γ_{ow} are the oil–air interface tension, water–air interface tension, and oil-water interface tension, respectively. θ_o, θ_w, and θ_{ow} are the contact angles of oil in air, water in air, and oil in water, respectively. From eqn (1) we are able to obtain confirmation that a hydrophilic surface in air that becomes oleophobic in water.[34]

After the introduction of micro/nanoscale hierarchical rough structure, a broad Cassie state can be achieved in the oil–water–solid system. When such surfaces are immersed in water, water can easily enter into the microstructures and occupy all interspaces between the microstructure on the surfaces, and be trapped among the micro/nanostructures. The oil droplet will reside on a composite solid–water interface, forming an oil–water–solid system, as shown in Fig. 6b. The water, which fills the interspaces between the oil droplet and the as-prepared surface, is an ideal superoleophobic material and results in the underwater superoleophobicity. The high oil contact angle can be explained by the generalized Cassie's equation:[32,33]

$$\cos\theta^*_{ow} = f\cos\theta_{ow} + f - 1 \quad (2)$$

where f is the area fraction of the projected oil wet area, θ_{ow} is the oil contact angle on a flat surface in water, and θ^*_{ow} is the contact angle of an oil droplet on a rough surface in water. In our experiment, θ_{ow} was 124.6 ± 1° when a 1,2-dichloroethane droplet was in contact with flat silicon in water. For the femtosecond laser structured surface, the oil droplet contacts only a

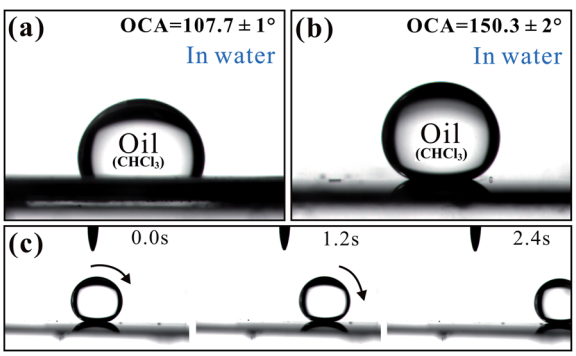

Fig. 5 Superoleophobicity and ultralow oil-adhesion of the as-prepared surface. (a) Shape of a chloroform droplet on the flat surface. (b) Shape of a chloroform droplet on the as-prepared rough surface. (c) Time sequence of snapshots of a chloroform droplet rolling on the 1° tilted surface.

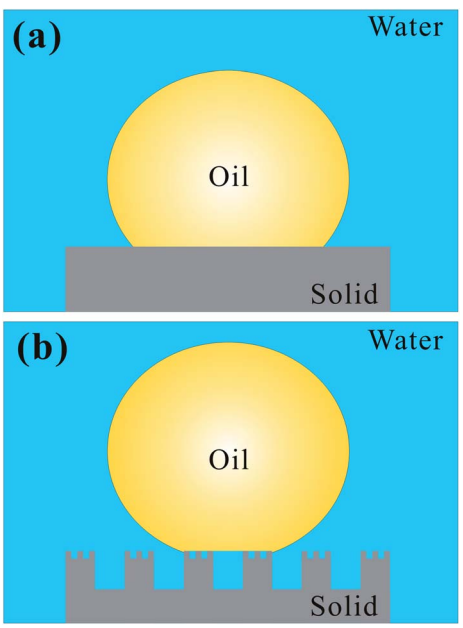

Fig. 6 Diagrams illustrating the effect of surface structure on the wetting behavior of solid substrates in an oil–water–solid three-phase system. An oil droplet on (a) a flat surface and (b) a micro/nanostructured surface in the water phase.

Published on 09 April 2014. Downloaded by Xian Jiaotong University on 04/11/2015 03:22:23.

small area of the surface, and the value of f can be inferred to be about 0.111 according to our previous work.[37] Therefore, we can calculate θ^*_{ow} according to eqn (2) and the value is close to 162° for a 1,2-dichloroethane droplet. The theoretical calculation agrees well with the measured value. Using the same procedure, the calculated value of θ^*_{ow} of a chloroform droplet is about 157°, fitting our experimental result very well. According to Cassie's model, the oil droplet sits on the conical spike forest, and water is trapped below the oil droplet. The water trapped in the hierarchical rough structure is a repulsive liquid phase for oil, giving rise to its superoleophobic property. On the other hand, the hierarchical microstructure can effectively reduce the contact area between the silicon surface and the oil droplet. As a result, the as-prepared surface shows a small adhesive force and ultralow oil adhesion. From the above analysis, it is concluded that hydrophilicity in air results in underwater oleophobicity, whereas the hierarchical rough structure can significantly amplify the superoleophobicity.

The situation where water mixes with an oily impurity is common in the pipes of household kitchens, and the drainage pipes are often blocked by an oily dirt. At present, the underwater superoleophobic surface with ultralow oil-adhesion provides a promising way to solve this problem. Fig. 7a shows the schematic of water with an oil impurity flowing in a conventional pipe. Because of the large contact area between the oil and pipe surface, which results in high oil adhesion, the oil impurity may stick closely to the inner wall of the pipe. On the one hand, the adherent oil droplet changes the tendency of water to move. The speed of water flow will diminish significantly, proceeding in an irregular course, making draining water less efficient. On the other hand, the adherent oil droplet can come into contact with other free oil impurities and form a larger one. After some time, the adherent oil accumulation grows to a certain size that will block the pipe. The blockage of drainage pipes causes a lot of inconvenience and problems in daily life. However, if the inner wall of the pipe shows superoleophobicity and ultralow oil-adhesion, the oil impurity droplet will roll forward along with the flow of water, as shown in Fig. 7b. In this way, the oil impurity's influence on the movement tendency of the water reaches a minimum, and the drainage pipes can remain working at high performance for an extended period of time. The oil-induced blockage is prevented because the impurity is taken away in time. This anti-blocking function can also be widely used in other fields; tissue engineering is just one example. If the artificial blood vessels possess underwater superoleophobicity, the probability that vascular obstruction occurs will be greatly reduced.

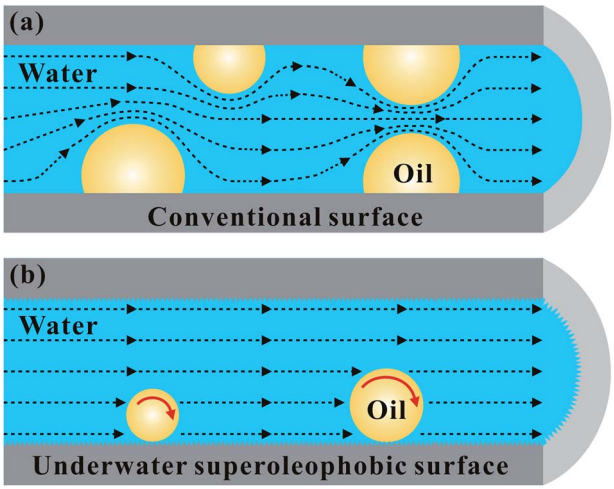

Fig. 7 Schematics of the effect of an underwater superoleophobic surface on preventing water pipe blocking by oily impurities. (a) Water with oily impurities flows in a conventional pipe. (b) Water with oily impurities flows in an underwater superoleophobic pipe. The black dotted lines express the movement tendency of the water. The red arrows indicate that the oily impurity droplet can roll forward along with the flow of water.

4. Conclusions

In summary, inspired by the scales of fish, an underwater superoleophobic surface was prepared by femtosecond laser microfabrication on silicon. The laser-induced surface shows micro/nanoscale hierarchical structure. The oleophobic properties of the as-prepared surface and underlying mechanisms were systematically investigated. The oil contact angles can reach up to 159.4 ± 1° and 150.3 ± 2°, respectively, for 1,2-dichloroethane and chloroform droplets in water. In addition, the surface shows ultralow oil adhesion. The sliding angles are only about 0.5° and 1°, respectively, for the 1,2-dichloroethane and chloroform droplets. In an oil–water–solid three-phase system, water can be trapped in the hierarchically rough structures and form a repulsive oil layer. The contact area between the as-prepared surface and the oil droplet is significantly reduced, resulting in superoleophobicity and low oil adhesion in water. The method we present here is simple and can accurately control the processing location, which may have widely potential applications in, for instance, microfluidics, biotechnologies, and antifouling coatings.

Acknowledgements

This work is supported by the National Science Foundation of China under the Grant no. 61275008 and 51335008, the Special-funded program on national key scientific instruments and equipment development of China under the Grant no. 2012YQ12004706.

References

1 F. Xia and L. Jiang, *Adv. Mater.*, 2008, **20**, 2842–2858.
2 T. L. Sun and G. Y. Qing, *Adv. Mater.*, 2011, **23**, H57–H77.
3 K. S. Liu and L. Jiang, *Annu. Rev. Mater. Res.*, 2012, **42**, 231–263.
4 K. S. Liu and L. Jiang, *Nano Today*, 2011, **6**, 155–175.
5 X. Yao, Y. L. Song and L. Jiang, *Adv. Mater.*, 2011, **23**, 719–734.
6 Y. L. Zhang, H. Xia, E. Kim and H. B. Sun, *Soft Matter*, 2012, **8**, 11217–11231.

This journal is © The Royal Society of Chemistry 2014

Published on 09 April 2014. Downloaded by Xian Jiaotong University on 04/11/2015 03:22:23.

7 Y. L. Zhang, Q. D. Chen, Z. Jin, E. Kim and H. B. Sun, *Nanoscale*, 2012, **4**, 4858–4869.
8 Y. B. Zhang, Y. Chen, L. Shi, J. Li and Z. G. Guo, *J. Mater. Chem.*, 2012, **22**, 799–815.
9 X. F. Gao and L. Jiang, *Nature*, 2004, **432**, 36.
10 X. Deng, L. Mammen, Y. Zhao, P. Lellig, K. Müllen, C. Li, H. J. Butt and D. Vollmer, *Adv. Mater.*, 2011, **23**, 2962–2965.
11 Y. Li, L. Li and J. Q. Sun, *Angew. Chem.*, 2010, **122**, 6265–6269.
12 W. Barthlott and C. Neinhuis, *Planta*, 1997, **202**, 1–8.
13 V. Zorba, E. Stratakis, M. Barberoglou, E. Spanakis, P. Tzanetakis, S. H. Anastasiadis and C. Fotakis, *Adv. Mater.*, 2008, **20**, 4049–4054.
14 J. L. Yong, Q. Yang, F. Chen, D. S. Zhang, G. Q. Du, J. H. Si, F. Yun and X. Hou, *J. Micromech. Microeng.*, 2014, **24**, 035006.
15 Q. F. Cheng, M. Z. Li, Y. M. Zheng, B. Su, S. T. Wang and L. Jiang, *Soft Matter*, 2011, **7**, 5948.
16 L. Feng, S. H. Li, Y. S. Li, H. J. Li, L. J. Zhang, J. Zhai, Y. L. Song, B. Q. Liu, L. Jiang and D. B. Zhu, *Adv. Mater.*, 2002, **14**, 1857–1860.
17 T. K. Wong, S. H. Kang, S. K. Y. Tang, E. J. Smythe, B. D. Hatton, A. Grinthal and J. Aizenberg, *Nature*, 2011, **477**, 443–446.
18 W. Barthlott, T. Schimmel, S. Wiersch, K. Koch, M. Brede, M. Barczewski, S. Walheim, A. Weis, A. Kaltenmaier, A. Leder and H. F. Bohn, *Adv. Mater.*, 2010, **22**, 2325–2328.
19 X. F. Gao, X. Yan, X. Yao, L. Xu, K. Zhang, J. H. Zhang, B. Yang and L. Jiang, *Adv. Mater.*, 2007, **19**, 2213–2217.
20 M. Motornov, R. Sheparovych, R. Lupitskyy, E. MacWilliams and S. Minko, *Adv. Mater.*, 2008, **20**, 200–205.
21 G. McHale, N. J. Shirtcliffe, C. R. Evans and M. I. Newton, *Appl. Phys. Lett.*, 2009, **94**, 064104.
22 Y. K. Lai, Y. X. Tang, J. J. Gong, D. G. Gong, L. F. Chi, C. J. Lin and Z. Chen, *J. Mater. Chem.*, 2012, **22**, 7420–7426.
23 N. J. Shirtcliffe, G. McHale, M. I. Newton and Y. Zhang, *ACS Appl. Mater. Interfaces*, 2009, **1**, 1316–1323.
24 A. Tuteja, W. Choi, M. Ma, J. M. Mabry, S. A. Mazzella, G. C. Rutledge, G. H. McKinley and R. E. Cohen, *Science*, 2007, **318**, 1618–1622.
25 X. Deng, L. Mammen, H. Butt and D. Vollmer, *Science*, 2012, **335**, 67–70.
26 K. Li, J. Ju, Z. X. Xue, J. Ma, L. Feng, S. Gao and L. Jiang, *Nat. Commun.*, 2013, **4**, 2276.
27 Z. X. Xue, Y. Z. Cao, N. Liu, L. Feng and L. Jiang, *J. Mater. Chem. A*, 2014, **2**, 2445–2460.
28 Y. Huang, M. J. Liu, J. X. Wang, J. M. Zhou, L. B. Wang, Y. L. Song and L. Jiang, *Adv. Funct. Mater.*, 2011, **21**, 4436–4441.
29 X. L. Liu, J. Zhou, Z. X. Xue, J. Gao, J. X. Meng, S. T. Wang and L. Jiang, *Adv. Mater.*, 2012, **24**, 3401–3405.
30 L. P. Xu, J. Zhao, B. Su, X. L. Liu, J. T. Peng, Y. B. Liu, H. L. Liu, G. Yang, L. Jiang, Y. Q. Wen, X. J. Zhang and S. T. Wang, *Adv. Mater.*, 2013, **25**, 606–611.
31 Q. F. Cheng, M. Z. Li, F. Yang, M. J. Liu, L. Li, S. T. Wang and L. Jiang, *Soft Matter*, 2012, **8**, 6740–6743.
32 D. Wu, S. Z. Wu, Q. D. Chen, S. Zhao, H. Zhang, J. Jiao, J. A. Piersol, J. N. Wang, H. B. Sun and L. Jiang, *Lab Chip*, 2011, **11**, 3873–3879.
33 Z. J. Cheng, H. Lai, Y. Du, K. W. Fu, R. Hou, N. Q. Zhang and K. N. Sun, *ACS Appl. Mater. Interfaces*, 2013, **5**, 11363–11370.
34 M. J. Liu, S. T. Wang, Z. X. Wei, Y. L. Song and L. Jiang, *Adv. Mater.*, 2009, **21**, 665–669.
35 L. Lin, M. J. Liu, L. Chen, P. P. Chen, J. Ma, D. Han and L. Jiang, *Adv. Mater.*, 2010, **22**, 4826–4830.
36 S. T. Wang and L. Jiang, *Adv. Mater.*, 2007, **19**, 3423–3424.
37 J. L. Yong, Q. Yang, F. Chen, D. S. Zhang, H. Bian, Y. Ou, J. H. Si, G. Q. Du and X. Hou, *Appl. Phys. A*, 2013, **111**, 243–249.
38 F. Zhang, W. B. Zhang, Z. Shi, D. Wang, J. Jin and L. Jiang, *Adv. Mater.*, 2013, **25**, 4192–4198.
39 Z. X. Xue, S. T. Wang, L. Lin, L. Chen, M. J. Liu, L. Feng and L. Jiang, *Adv. Mater.*, 2011, **23**, 4270–4273.
40 X. L. Liu, J. Gao, Z. X. Xue, L. Chen, L. Li, L. Jiang and S. T. Wang, *ACS Nano*, 2012, **6**, 5614–5620.
41 Q. Wen, J. C. Di, L. Jiang, J. H. Yu and R. R. Xu, *Chem. Sci.*, 2013, **4**, 591–595.
42 M. H. Jin, S. S. Li, J. Wang, Z. X. Xue, M. Y. Liao and S. T. Wang, *Chem. Commun.*, 2012, **48**, 11745–11747.
43 Q. Zhu, Q. M. Pan and F. T. Liu, *J. Phys. Chem. C*, 2011, **115**, 17464–17470.
44 F. Chen, D. S. Zhang, Q. Yang, J. L. Yong, G. Q. Du, J. H. Si, F. Yun and X. Hou, *ACS Appl. Mater. Interfaces*, 2013, **5**, 6777–66792.
45 J. L. Yong, Q. Yang, F. Chen, D. S. Zhang, U. Farooq, G. Q. Du and X. Hou, *J. Mater. Chem. A*, 2014, **2**, 5499–5507.
46 J. L. Yong, Q. Yang, F. Chen, D. S. Zhang, G. Q. Du, H. Bian, J. H. Si and X. Hou, *RSC Adv.*, 2014, **4**, 8138–8143.
47 D. S. Zhang, F. Chen, Q. Yang, J. H. Si and X. Hou, *Soft Matter*, 2011, **7**, 8337–8342.
48 J. L. Yong, F. Chen, Q. Yang, D. S. Zhang, H. Bian, G. Q. Du, J. H. Si, X. W. Meng and X. Hou, *Langmuir*, 2013, **29**, 3274–3279.
49 J. L. Yong, F. Chen, Q. Yang, D. S. Zhang, G. Q. Du, J. H. Si, F. Yun and X. Hou, *J. Phys. Chem. C*, 2013, **117**, 24907–24912.
50 D. S. Zhang, F. Chen, Q. Yang, J. L. Yong, H. Bian, Y. Ou, J. H. Si, X. W. Meng and X. Hou, *ACS Appl. Mater. Interfaces*, 2012, **4**, 4905–4912.
51 F. Chen, D. S. Zhang, Q. Yang, X. H. Wang, B. J. Dai, X. M. Li, X. Q. Hao, Y. C. Ding, J. H. Si and X. Hou, *Langmuir*, 2011, **27**, 359–365.
52 J. L. Yong, F. Chen, Q. Yang, G. Q. Du, H. Bian, D. S. Zhang, J. H. Si, F. Yun and X. Hou, *ACS Appl. Mater. Interfaces*, 2013, **5**, 9382–9385.
53 J. L. Yong, Q. Yang, F. Chen, D. S. Zhang, G. Q. Du, H. Bian, J. H. Si, F. Yun and X. Hou, *Appl. Surf. Sci.*, 2014, **288**, 579–583.
54 F. Chen, H. W. Liu, Q. Yang, X. H. Wang, C. Hou, H. Bian, W. W. Liang, J. H. Si and X. Hou, *Opt. Express*, 2010, **18**, 20334–20343.
55 S. G. He, F. Chen, K. Y. Liu, Q. Yang, H. W. Liu, H. Bian, X. W. Meng, C. Shan, J. H. Si, Y. L. Zhao and X. Hou, *Opt. Lett.*, 2012, **37**, 3825–3827.
56 T. Her, R. J. Finlay, C. Wu, S. Deliwala and E. Mazur, *Appl. Phys. Lett.*, 1998, **73**, 1673–1675.
57 M. Y. Shen, C. H. Crouch, J. E. Carey and E. Mazur, *Appl. Phys. Lett.*, 2004, **85**, 5694–5696.